Available online at www.sciencedirect.com
SCIENCE DIRECT
Journal of Organometallic Chemistry 691 (2006) 267–281
Journal of Organometallic Chemistry
www.elsevier.com/locate/jorganchem

An experimental and DFT computational study of a novel zerovalent tetracarbonyl tungsten complex of 2-(2′-pyridyl)quinoxaline

Irene Veroni [a], Christodoulos Makedonas [a], Aliki Rontoyianni [b], Christiana A. Mitsopoulou [a,*]

[a] *Inorganic Chemistry Laboratory, Department of Chemistry, National and Kapodistrian University of Athens, Panepistimiopolis, Zografou 15771, Hellas, Greece*
[b] *Physical Chemistry Laboratory, Department of Chemistry, National and Kapodistrian University of Athens, Panepistimiopolis, Zografou 15771, Hellas, Greece*

Received 10 May 2005; received in revised form 25 June 2005; accepted 4 July 2005
Available online 2 December 2005

Abstract

Synthesis and characterization of the new complex $W(CO)_4$(2,2′-pq), (**1**), where 2,2′-pq = 2-(2′-pyridyl)quinoxaline, is presented. The non-symmetric ligand 2,2′-pq belongs to the general class of quinoxalines, which are natural products yielding a rich coordination chemistry. Complex (**1**) crystallizes in space group $P2_{1/n}$ with $a = 9.601(6)$ Å, $b = 16.735(11)$ Å, $c = 10.315(8)$ Å, $Z = 4$ and $V = 1616.0(19)$ Å^3. Although its structure resembles those of $W(CO)_4$(phen) and $W(CO)_4$(bpy), some distortions that stem from 2,2′-pq's asymmetry are present. DFT calculations reveal a ground state consisting of HOMO, HOMO − 1 and HOMO − 2, mainly of metal and carbonyl character, while LUMO is diimine oriented. The bonding scheme of (**1**) is illustrated after its consideration as been consisted by two fragments, namely $W(CO)_4$ and 2,2′-pq, acting as a donor and acceptor of electron density, respectively. In that scheme, back-bonding interaction of the main core to 2,2′-pq is mainly related to the mixing of HOMO − 2 from $W(CO)_4$ moiety with LUMO from 2,2′-pq moiety. The performed TDDFT calculations, not only in the gas phase but also combined with the conductor like polarizable continuum model (CPCM), reveal that the lowest in energy highly solvatochromic transition of (**1**) can be ascribed as a HOMO − 2 → LUMO transition and it is better described as MLCT/LLCT, underlying the CO → diimine contribution. The solvatochromic behaviour of (**1**) is anticipated by DFT/CPCM calculations and is probed in detail by absorption and NMR spectroscopy. The correlation of the lowest-energy-band maximum to the dipole moment of the corresponding solvents provides overall good linear fits, while the correlation to the dielectric constant affords good linear patterns only after the segregation of the solvents into groups. The ^{1}H NMR data of 2,2′-pq and (**1**) reveal an increase of the solvent influence to the chemical shifts of the diimine ligand after its coordination to the metal and suggest two different types of solvent-effects for the complex and the ligand, respectively. The observed proton shifts of (**1**) are related with the results of the Mülliken population analysis in solvents of different polarity; the transition from CCl_4 to MeOH seems to signify a charge transfer from the axial COs and the central metal to the equatorial COs and the internal nuclei of 2,2′-pq.

Keywords: 2-(2′-pyridyl)quinoxaline; Tetracarbonyl; Tungsten; DFT; TDDFT; Solvatochromism

1. Introduction

During the last 50 years, the $M(CO)_4L$-type (M: Cr, Mo, W and L: O, N, S, P donor bidentate ligand) complexes have been very common synthons in most synthetic laboratories while a great number of compounds

* Corresponding author. Tel.: +30 2107274452; fax: +30 2108322828.
E-mail address: cmitsop@chem.uoa.gr (C.A. Mitsopoulou).

0022-328X/$ - see front matter © 2005 Elsevier B.V. All rights reserved.
doi:10.1016/j.jorganchem.2005.07.023

have emanated from them, through thermal or photochemical reactions [1]. The information about their structure and properties was growing along with the development mainly of IR, Raman and fluorescence spectroscopies; the first two could indirectly provide an insight into the electronic distribution in their ground state and of spectroscopy, while the latter could elucidate their excited states by explaining the nature of their dual emission [2]. The interest in these model-complexes was reanimated after the recent publications by Vlček et al. who carried out several DFT calculations on certain complexes of this family and overthrew some misunderstandings of the past [3]. In parallel to the reconsideration of some of their properties, several practical applications of these complexes originating from their photophysical characteristics are currently being tested; they are considered as candidates for probes in polymerization processes [4], in the labeling of biomolecules [5] and in the exploitation of solar energy [6]. Quite prominent could also be their use as NLO materials, due to their MLCT transitions, which may give rise to large microscopic second-order non-linearities (β_{ijk}) [7].

Herein, the solvatochromic behavior of a non-symmetric tetracarbonyl complex W(CO)$_4$(2,2′-pq) (**1**), where 2,2′-pq stands for 2-(2′-pyridyl)quinoxaline (Scheme 1), is studied by means of DFT and TD-DFT calculations. Furthermore, the solvatochromic behavior of (**1**) was monitored in a series of solvents, so as to gain an insight in the solvation mechanisms that could affect its properties. We have recorded the maxima of the solvatochromic low energy band of (**1**) in various solvents and have tried to correlate them with the dielectric constant and the dipole moment of the solvents. Moreover, we have measured and interpreted the ^{1}H NMR spectra of both the complex and the ligand in several different solvents, observing the effect of the *solvent reaction field* [8] on the chemical shifts. DFT calculations using solvent cages of different polarity have been employed to substantiate some of our arguments about solvatochromism.

The synthesis, the crystal structure and the spectroscopic features of (**1**) is also presented. The selection of the metal (W vs. Mo) has been made having in mind the recent studies on W complexes and the convenience in comparing it to literature results. The choice of 2,2′-pq as a diimine-ligand is quite challenging due to the high importance of the class where it belongs; quinoxalines are natural products [9] and are used as antibiotics [10]. They can also form polymers with peculiar magnetic and electric properties [11]. Moreover, their significant redox chemistry and photochemistry are responsible for many considerable intra- and inter-electron transfer organic and biochemical processes [12]. From a different point of view, the choice of 2,2′-pq is quite stimulating because it is a non-symmetric ligand, in contrast to the majority of the α-diimines that have been complexed on the W(CO)$_4$ moiety; the study of the tetracarbonyl complex (**1**) and its comparison to analogous symmetric ones is expected to be enlightening. DFT calculations that are currently used in many classes of compounds, so as to reveal and interpret their properties [13], are utilized here and shed light on the electronic distribution of (**1**) in energy levels. By using the notation of a donor and an acceptor part inside (**1**)'s structure, a fragment orbital analysis is applied separately to the W(CO)$_4$ and 2,2′-pq moiety, which are finally combined to afford its bonding scheme in a unique way. The absorption spectrum of (**1**) is also reproduced and explained by TDDFT calculations in the gas phase, whereas the solvation of the states that are tightly connected to the highly solvatochromic band is considered by the tandem use of TDDFT and CPCM models. The latter is being performed for the first time for W(diimine)(CO)$_4$ compounds.

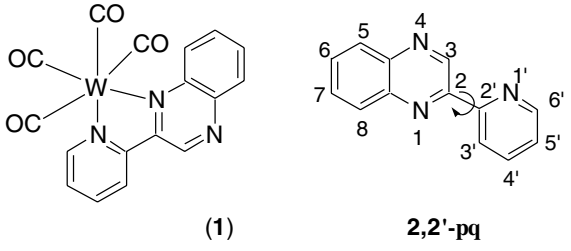

Scheme 1.

2. Experimental

2.1. Materials

2,2′-pq was synthesized following Hadjiliadis routine [14]. The complex W(CO)$_6$ along with THF, which was used in syntheses, were obtained from Aldrich Chemicals and used after being dried. The solvents used in UV–visible studies were purified to spectroscopic quality by standard methods [15]. The deuterated solvents, which were utilized in NMR experiments, were purchased from Aldrich and were of 99.99% purity.

2.2. Instrumentation

Photolysis experiment was carried out with a 1000 W Xenon lamp in an Oriel, mod 68820, Universal Arc. Lamp source selected with appropriate interference filter (Corning). FT-IR spectra in solution and in KBr pellets were recorded on a Nicolet Magna IR 560 spectrophotometer having 1.0 cm^{-1} resolution. Electronic absorption spectra were recorded on a Varian Cary 300 spectrometer at 25 ± 0.2 °C. The solute concentration was ≈10^{-5} M and the samples were prepared just before the measurements. ^{1}H NMR measurements were

performed using a Varian Unity Plus 300 NMR spectrometer. Samples were run in a 5 mm probe with deuterated solvents as internal lock and reference. The assignment of the ^{1}H NMR spectra of the free ligand L and of the complexes is based on 2D NMR experiments (^{1}H–^{1}H COSY). Microanalyses were performed with a Euro Vector EA 3000 analyzer.

2.3. Synthesis of $W(CO)_4$(2,2′-pq) (1)

A deoxygenated solution of $W(CO)_6$ (0.352 g, 1.00 mmol) in THF (25 mL) was irradiated with a 1000 W Xenon lamp at 25 °C for 30 min. To the bright yellow solution that came along after the irradiation, we added the ligand 2,2′-pq (0.378 g, 1.00 mmol) and the solution was stirred and heated at 50 °C for 8 h. At the end, the solvent was removed with a rotary evaporator and the dark purple residue was collected, washed successively with 3 ml of hot methanol and twice with 5 ml portions of *n*-heptane and dried in vacuum. (yield: 45%). Anal. Calc.: C, 40.58; H, 1.80; N, 8.35. Found: C, 41.03; H, 1.78; N, 8.29%.

2.4. X-ray crystallography of (1)

Crystal data and details of data collection are given in Table 1. The dark purple, prismatic crystals suitable for X-ray structural determination were obtained by recrystallization during slow evaporation from a mixture of *n*-hexane-dichloromethane (4:1) at 279 K. Unit cell parameters were calculated from 30 reflections. Crystallographic data were collected on a Syntex $P2_1$ diffractometer with graphite monochromated Cu Kα radiation at room temperature (293 K). Absorption and decay correction was applied. A total of 2294 reflections were used in further calculations. The structure was solved by direct methods SHELXS [16] program package. Full-matrix least-squares anisotropic refinement for all non-hydrogen atoms, yielded $R = 0.0786$, $R_w = 0.2141$ and $S = 1.067$. The structure of (**1**) produced by ORTEP3 for Windows [17] is presented in Fig. 1.

2.5. Computational details

Ground-state electronic structure calculations of (**1**) have been performed using density functional theory (DFT) [18] methods employing the GAUSSIAN-1998 software package [19]. The functional used throughout this study is the B3LYP, consisting of a hybrid exchange functional as defined by Becke's three-parameter equation [20] and the non-local Lee–Yang–Parr correlation functional [21]. The ground state geometries were obtained in the gas phase by full geometry optimization, starting from structural data. The optimum structures located as saddle points on the potential energy surfaces, were verified by the absence of imaginary frequencies. The derived wavefunctions were found free of internal instabilities. The basis set used throughout this study is the full double-ζ LANL2DZ basis functions together with the corresponding effective core potential for tungsten [22]. In order to estimate the possible response of electronic structure due to the solvation, the solvent was modeled by the polarizable conductor calculation model (CPCM) as implemented in G98 [23]. We set the α-parameter at the value of 1.3 and used 80 tessarae per sphere when defining the cavity, since tighter option may result in charge penetration into the cavity. Percentage compositions of molecular orbitals from the four contributing fragments (the metal, the 2,2′-pq, the axial and the equatorial carbonyls) were calculated and analyzed using the AOMix and AOMix-CDA programs [24], with the latter being extensively used for the fragments molecular orbital (FMO) analysis. The first 21 singlet excited states of the closed shell complexes were calculated within the TDDFT formalism

Table 1
Crystallographic data for compound (**1**)

Formula	$C_{17}H_9N_3O_4W$
M	503.12
Crystal system	Monoclinic
Space group	$P2_1/c$
a (Å)	9.601(6)
b (Å)	16.735(11)
c (Å)	10.315(8)
β (°)	102.82(3)
V (Å^3)	1616.0(19)
T (K)	293
Z	4
Total number of data	2294
Reflections $I > 2\sigma I$	2060
R_{int}	0.1240
R	0.0786
wR	0.2141

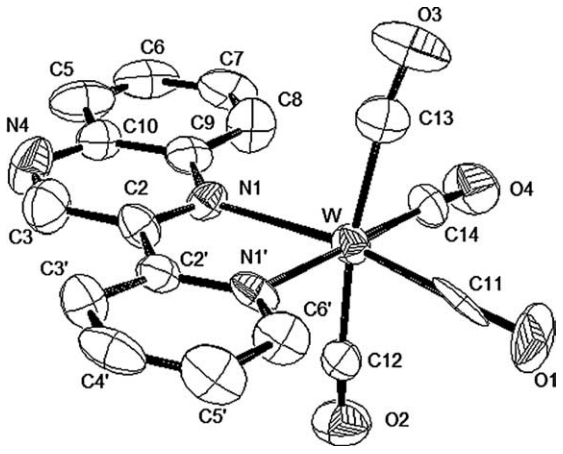

Fig. 1. An ORTEP drawing of complex (**1**) with the atomic numbering scheme.

[25]. Moreover, non-equilibrium TDDFT/CPCM calculations, as implemented in the GAUSSIAN-03 [26] program package, were employed in order to reproduce the solvation of the lowest states that are involved in the main highly solvatochromic band of (**1**) in two solvents of different polarity, namely methanol and carbon tetrachloride. The percentage of different transitions contributing to a state were calculated with the aid of SWizard [27]. Finally, regression analyses were carried out using the commercial StatGraphics Plus 4.0 software package.

3. Results and discussion

The synthetic procedure of (**1**) was based on the method of Strohmeier and Müller [28], which involves UV irradiation of tungsten hexacarbonyl in tetrahydrofuran and subsequent addition of the ligand (Scheme 2). The first reaction step (Scheme 1) is related to the photochemical dissociation of one M–CO bond and the complexation of one molecule of THF solvent, while the thermal reaction step involves the substitution of THF from 2,2′–pq and its chelation on the metal center (Scheme 1). The overall reactions can be considered as quite clean and afford (**1**) in a good yield.

Single crystals of the corresponding complex (**1**), suitable for X-ray crystallography, were grown by slow evaporation in a *n*-hexane:dichloromethane (4:1) solution. As shown in the crystallographic structure of (**1**) in Fig. 1, it exhibits distorted octahedron geometry with the metal atom bonded to four carbonyls and a bidentate ligand, the latter possessing, two N atoms as donors. In Table 2, the most important bond lengths and angles are displayed. The distances within the coordinated 2-(2′-pyridyl)quinoxaline in (**1**) are in good correlation with the corresponding ones in the free ligand [29] and in a number of 2-(2′-pyridyl)quinoxaline complexes with different metals [30,31].

The small angle of N_1–W–$N_{1'}$(72.48°) and the bending of the axial carbonyls away from the diimine ligand of 2,2′-pq (the angle C_{13}–W–C_{12} equals to 170.1° instead of 180°) are two characteristics well considered in the literature for this family of complexes [32]. While for the first one the reason could be steric, the second should originate from electronic reasons. Further, the Os' bend out of the W–C bonds is also a common but rather underestimated trend of all complexes of this class. On

$$W(CO)_6 \xrightarrow[THF]{h\nu} W(CO)_5(THF) \quad (1)$$

$$W(CO)_5(THF) + 2,2'\text{ pq} \xrightarrow{50^0C} W(CO)_4(2,2'\text{ pq}) \quad (2)$$

Scheme 2.

Table 2
Selected molecular parameters (distances in Å, angles in deg.) of compound (**1**)

Atomic distances (Å)		Atomic angles (°)	
W–N_1	2.299(10)	N_1–W–N_1'	72.7(4)
W–N_1'	2.202(10)	C_{12}–W–C_{13}	170.1(6)
W–C_{11}	1.944(19)	W–C_{12}–O_2	175.9(13)
W–C_{12}	2.008(16)	W–C_{13}–O_3	173.5(16)
W–C_{13}	2.012(17)	C_{11}–W–C_{14}	88.6(6)
W–C_{14}	1.989(14)	W–C_{11}–O_1	177.5(13)
C_{11}–O_1	1.19(2)	W–C_{14}–O_4	176.7(14)
C_{12}–O_2	1.157(19)	N_1–W–C_{14}	107.0(5)
C_{13}–O_3	1.16(2)	N_1'–W–C_{11}	91.7(5)
C_{14}–O_4	1.134(17)	N_1–W–C_{13}	93.8(5)
C_2–C_2'	1.460(18)	N_1'–W – C_{13}	94.9(5)
N_1–C_2	1.310(17)	N_1–W–C_{12}	93.4(5)
N_1'–C_2'	1.367(17)	N_1'–W–C_{12}	93.8(4)

the other hand, the bond W–N_1 is 0.10 Å longer than the W–N_1', something that is probably due to the steric effect, which is imposed by the Ph-ring of the quinoxaline moiety and implies a stronger bonding of W to the pyridyl than to the quinoxaline moiety of the ligand. The latter may be connected to the larger distance of W–C_{14} compared to W–C_{11}. An observation consistent to the trans influence effect. On the axial plane, the bonds W–C_{ax} are longer than the bonds W–C_{eq} on the equatorial plane, as a result of the smaller π-acidity of 2,2′-pq compared to that of COs. In parallel, the bonds $(C–O)_{ax}$ are shorter than the bond C_1–O_{11} on the equatorial plane, but paradoxically slightly longer than the bond C_{14}–O_4 *trans* to the pyridyl moiety of the ligand.

Despite the overall similarity of the structures of (**1**) and the rest reported symmetrical tetracarbonyl complexes, there are some crucial details that differentiate (**1**). One of them is the above-mentioned differences between the W–N bond lengths; which may be the reason for the slight leaning of the axial carbonyls towards the quinoxaline part of the diimine. The strongest repulsion of the axial CO orbitals against the occupied orbitals of the pyridine moiety results in the formation of a dihedral angle with a value greater than 90°, which has not been referenced before for the symmetrical complexes of this class. In addition to these, the different values of the angles N_1'–W–C_{14}(= 179.5°) and N_1–W–C_{11}(=164.4°) as well as the non-orthogonal way that 2,2′-pq binds to the central metal, introduce extra asymmetries into (**1**)'s structure that can influence its properties.

The FT-IR spectrum obtained from (**1**) in CH_2Cl_2 (Fig. 2) in the CO stretching region, exhibits four bands at 2011 (A_1), 1906 (B_1), 1882 (A_1) and 1834 (B_2) cm^{-1}, while the corresponding vibrations of (**1**) taken in KBr pellets are 1995 (A_1), 1893 (B_1), 1856 (A_1) and 1817 (B_2) cm^{-1}; the symmetry assignments are given in accordance with previously reported data [33]. The mean value of the above four stretching CO frequencies as

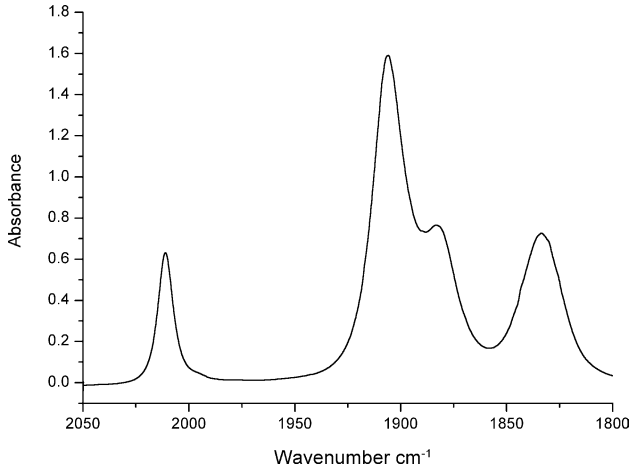

Fig. 2. FT-IR spectrum of (**1**) in CH_2Cl_2.

compared to the corresponding one of $W(CO)_4$phen complex, is slightly higher, which indicates a stronger back-donation to 2,2′-pq in comparison with phen.

The electronic absorption spectrum of (**1**) is similar to analogous complexes of this series [34] and is dominated by two intense absorption bands (Fig. 3). The first one is at the high energy side of the spectrum, at 332 nm ($\varepsilon = 9471\ M^{-1}\,cm^{-1}$ and spectral bandwidth of $\sim$4200 cm^{-1}) while the second one is at the lower energy side. The latter is solvent depended. Both bands are structured indicating that they conclude more than one transition. This is obvious in hexane solution where although (**1**) is slightly dissolved, provides us with a spectrum revealing much more bands, namely 325 nm (3.83 eV), 403 nm (3.08 eV), 418 nm (2.97 eV) in the high-energy band and 590 nm (2.09 eV) in the low energy band. The observed shoulder at the high energy side of the lower energy band is also solvent depended (Fig. 3, 3 vs. 1); in the polar solvents are usually hidden inside the main bands.

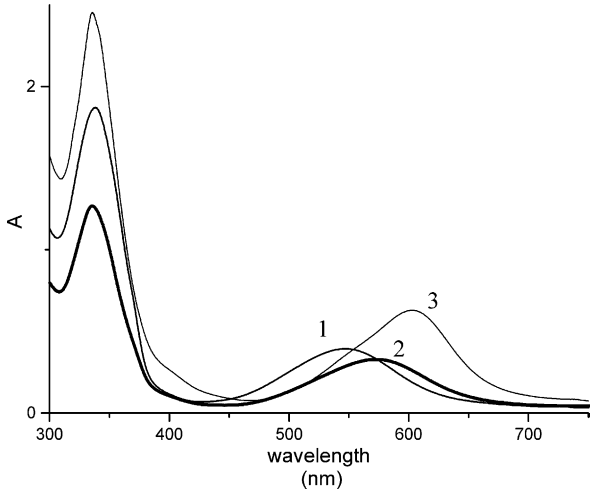

Fig. 3. Electronic absorption spectra of (**1**) in: CH_3CN (1), MeOH (2) and $(CH_3CH_2)_2O$ (3).

4. Theoretical results

4.1. Ground state structures and electronic description

DFT calculations were performed on complex (**1**) starting from crystallographic data (Table 3) in the gas phase and under the electric field of two solvents, CCl_4 and CH_3OH.

As it can be seen from Table 3 the overall agreement between theory and experiment is satisfactory. Based on both experimental and theoretical results, a few points should be stressed. Firstly, tungsten faces distorted octahedral coordination sphere, as expected. The bond W–N1 is 0.10 Å longer than the W–N1, showing the stronger bonding behavior of the pyridyl moiety as compared to the quinoxaline's. The induced trans influence from the N-donor is postulated by the W–C and C–O distances on the equatorial plane. Moreover, the characteristic bending of axial carbonyls away from the diimine ligand is also present here giving an $(OC)_{ax}$–W–$(CO)_{ax}$ angle of 170.1°. The overall accuracy of the calculations seems to be satisfactory based on the large estimated standard deviation's on the X-ray data. In any solvent, the largest deviation from the experiment comes in the reproduction of C–O distance of the carbonyl *trans* to pyridyl, which is overestimated; whereas the whole accuracy is depending on solvents' polarity.

The orbital energies along with the contributions from the ligands and the metal are given in Table 4. In the gas phase, the overall pattern is qualitatively similar to the symmetric complexes of the same type [3]. In the first place, taking into consideration Table 4 and Fig. 4

Table 3
Comparison of calculated selected bond lengths (Å) and angles (°) for (**1**) in the gas phase and two solvents with experimental values from X-ray analysis

C.I.	(1)			
M	Exp.	gp	CCl_4	CH_3OH
W–N1	2.299(10)	2.270	2.270	2.280
W–N1′	2.202(10)	2.215	2.216	2.223
W–C11	1.944(19)	1.969	1.964	1.960
W–C14	1.989(14)	1.980	1.973	1.966
W–C12	2.008(16)	2.036	2.031	2.028
W–C13	2.012(17)	2.036	2.031	2.028
C11–O1	1.19(2)	1.196	1.198	1.202
C14–O4	1.134(17)	1.196	1.199	1.205
C12–O2	1.157(19)	1.185	1.186	1.189
C13–O3	1.16(2)	1.185	1.186	1.189
$\phi_{dim.}$	72.7(4)	73.4	73.5	73.6
ϕ_{eq}	88.6(6)	88.0	87.7	86.8
ϕ_{ax}	170.1(6)	173.6	173.5	174.2

Table 4
Contribution of different fragments to complexes' valence orbitals

MO	E_{eV}	W	pq	CO_{eq}	CO_{ax}
Gas phase					
94	−1.41	16.7	−1.9	−0.5	85.7
93	−1.63	18.2	0.2	6.6	75.0
92	−2.20	0.6	97.0	1.7	0.7
91	−2.40	0.2	99.0	0.5	0.3
90	**−3.52**	**4.5**	**89.1**	**3.2**	**3.2**
89	**−5.51**	**63.3**	**1.3**	**34.9**	**0.5**
88	−5.76	58.1	4.8	14.1	23.0
87	−5.90	55.0	13.5	11.1	20.4
86	−7.53	0.9	98.7	0.1	0.3
85	−7.82	0.1	99.8	0.0	0.1
84	−7.98	1.0	98.1	0.8	0.1
CCl_4					
94	−1.53	16.0	−1.7	−0.5	86.3
93	−1.75	17.6	0.3	6.6	75.4
92	−2.0	0.5	96.9	2.0	0.6
91	−2.26	0.2	99.0	0.6	0.2
90	**−3.42**	**3.8**	**90.1**	**3.2**	**2.9**
89	**−5.65**	**62.5**	**1.2**	**35.8**	**0.5**
88	−5.88	57.2	5.4	14.4	23.1
87	−6.01	55.0	12.3	11.7	20.9
86	−7.44	1.1	98.4	0.2	0.3
85	−7.68	0.2	99.7	0.0	0.1
84	−7.90	1.0	98.1	0.8	0.1
CH_3OH					
94	−1.66	0.6	95.7	2.9	0.7
93	−1.68	15.0	−1.0	−0.6	86.6
92	−1.89	16.7	0.6	6.2	76.5
91	−2.03	0.2	99.1	0.6	0.2
90	**−3.23**	**2.3**	**92.9**	**2.9**	**2.0**
89	**−5.79**	**61.2**	**1.1**	**37.3**	**0.4**
88	−5.99	56.0	5.6	14.9	23.4
87	−6.12	55.3	10.3	13.0	21.4
86	−7.27	1.3	98.0	0.2	0.4
85	−7.46	0.4	99.3	0.1	0.1
84	−7.82	1.2	97.9	0.8	0.1

HOMO and LUMO orbitals are shown in bold.

where HOMOs and LUMOs are indicated, we notice that the three highest occupied molecular orbitals span very close in energy, with the major contributions coming from metal's d-orbitals (mainly d_{xz} in case of HOMO) and carbonyls' π* orbitals. The high diimine contribution in HOMO − 2 describes the M → diimine π back bonding, something that is common to all complexes of this class [3a], indicating that HOMO − 2 is spectroscopically the most important of the HOMO manifold. The main difference between the HOMO and the two HOMOs-1 and -2 is that the COs' character is not the same. HOMO is mainly dominated by the equatorial COs, while HOMOs-1,2 by the axial ones. The three highest occupied MOs could be compared to the t_{2g} set of MOs in $W(CO)_6$ concerning their π bonding character and having in mind that a splitting to a_1, a_2 and b_1 is caused by O_h symmetry. On the other hand, HOMO-3 to HOMO-5 are localized on 2,2′-pq and more specifically, HOMO-3 lies on the quinoxaline moiety, HOMO-4 lies on both moieties while HOMO-5 character is mainly dominated by N_4 *p* contribution.

LUMO is mainly localized on the five-member ring and is a combination of C_2, C_2', N_1 and N_1' orbitals. It corresponds to b_1^* orbital of bipyridine or phenanthroline in analogous complexes. LUMO + 1 and LUMO + 2 are very close in energy and are localized on 2,2′-pq; in particular, although LUMO + 1 lies on the whole bindate ligand, LUMO + 2 lies only on the pyridyl fragment. In contrast, both LUMO + 3 and LUMO+4 character arises from the axial carbonyls. The metal d_{xz} contribution to LUMO along with the W/diimine mixing in the HOMO − 2 is consistent with the π-back bonding theory. The latter plays an important role to complexes' optical properties.

Trying to gain more insight on the bonding scheme of (**1**), we envisioned the molecule as been consisted by two fragments, namely $W(CO)_4$ and 2,2′-pq, acting as a donor and acceptor of electron density, respectively [35]. The derived pattern of this fragment orbital analysis is manifested in Fig. 5 for HOMO − 2 to LUMO molecular orbitals. The molecular orbitals of the central unit $W(CO)_4$ are reported at the left side of the diagram, whereas those of the diimine are displayed at the right side. As it is indicated, HOMO and HOMO − 1 orbitals of the complex almost entirely originate from $W(CO)_4$ fragment, while LUMO is a combination of diimine's LUMO and metal-carbonyls' HOMO − 2 orbitals. This combination along with the HOMO − 2 character, are indicative of the back donation procedure. Being more precise, complex's HOMO − 2 is a mixture of 81.8% of $W(CO)_4$'s HOMO − 2 and 7.9% of 2,2′-pq's LUMO. This reveals the electron density donation path from the main core back to diimine in a total amount of 0.054 e^- (as extracted by the CDA software). An analogous treatment for the $W(CO)_4$phen complex yielded an amount of 0.022 e^- as back-donation to diimine in agreement with the IR experimental results.

In our study, the solvent's effect was modeled by the polarizable conductor calculation model (CPCM). Although Koopman's theorem does not apply to DFT and the energies of Kohn–Sham orbitals cannot be used as in the case of Hartee–Fock calculations, it is widely acceptable that the energy difference ΔE between the HOMO and the LUMO can be considered as a valuable parameter [36]. Based on that assumption, the applicability of the polarizable conductor calculation was tested recently [37] and proved that it can be used efficiently in the description of highly solvatochromic compounds, a fact justifying the following discussion.

The selected solvents were carbon tetrachloride and methanol based on criteria of polarity and compounds' solubility. The whole case is best described by Fig. 4. First of all, it is obvious that solvents' electric field stabilizes the orbitals that are localized on the metal and the carbonyl groups, destabilizing those with large

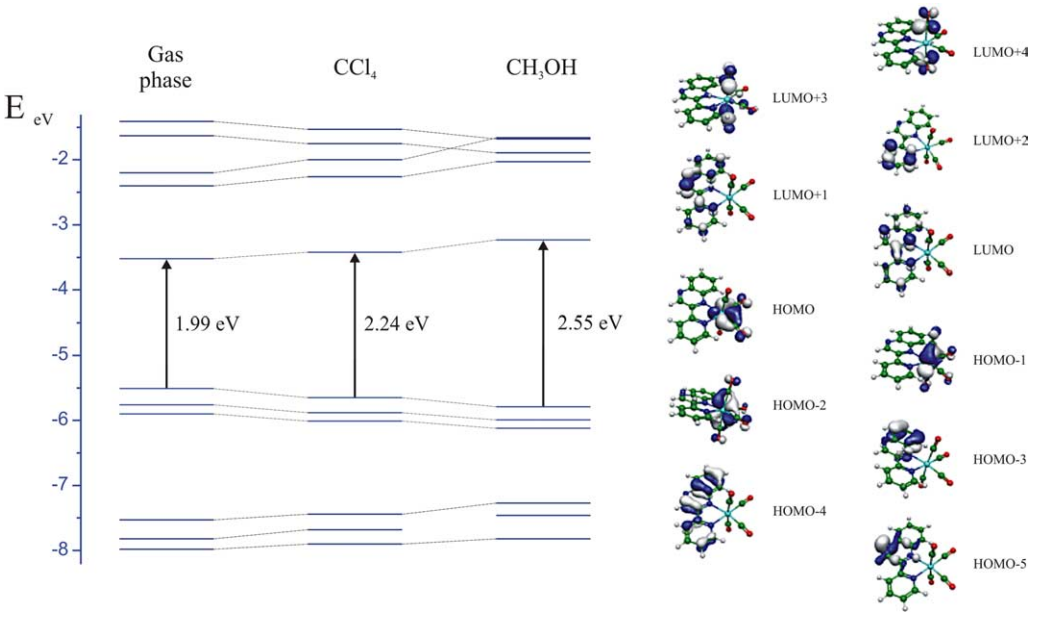

Fig. 4. Diagram of electronic energy levels of (**1**) corresponding to the gas phase, MeOH and CCl_4. Contour plots of valence orbitals extracted from the calculation in the gas phase are also presented.

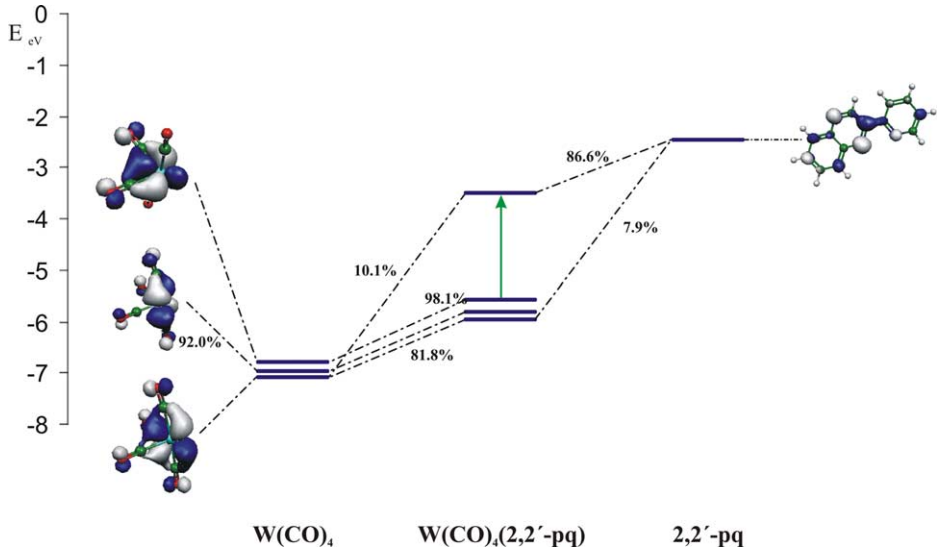

Fig. 5. Schematic representation of the way that the orbitals of $W(CO)_4$ moiety mix with the orbitals of diimine moiety, so as to form the orbitals of the complex (**1**).

diimine character. This trend enhances the HOMO–LUMO energy difference, in total accordance with the experimental result of negative solvatochromism and it also leads to the observed switching between LUMO + 2 and LUMO + 3 on going from CCl_4 to MeOH. This produces a charge delocalization in the ground state. In other words, solvation procedure, through the interactions between solvent's field and polar solute, mainly of the dipole–dipole character, stabilizes the orbitals localized on this part of the molecule with the higher electron density, destabilizing all the rest. In compounds of this type, electron density is centered mainly on the metal and carbonyl ligands. Although the difference in orbital energies are of the same magnitude as the observed band shifts, going from carbon tetrachloride to methanol ($\sim$1800 cm^{-1}), to better understand how solvation of ground and excited states alter the energetic levels and affect the solvatochromism of these compounds, we have undertaken TDDFT/CPCM calculations. The results are discussed in the next section.

Considering once again the fragments' contribution (Table 4) we conclude that metal's contribution to HOMO tends to diminish upon solvation and solvent's

polarity in favor of equatorial carbonyl's. The aforementioned statement holds true in general for tungsten. It is also noteworthy, that metal's and axial carbonyl's contribution to LUMO is reduced in favor of diimine's one; whereas the latter's contribution to HOMO − 2 is reduced in favor mainly of the carbonyls'. In other words, a slight trend of reduction in back donation from metal to diimine seems to be the case upon a raise in solvent's dielectric constant. This observation can be possibly employed in cases of ligand abstraction or replacement, either photochemically or chemically induced, where solvent's selection might be important.

Finally, it should be stressed that compound's ground state is anticipated to become less polar on going from polar to non-polar solvents as a direct consequence of negative solvatochromism. This conclusion is confirmed by our DFT calculations and the calculated complexes' dipole moment in methanol (13.88 D) and in carbon tetrachloride (10.79 D).

4.2. Excited states and absorption spectra

In order to investigate the lowest lying singlet states of (**1**), TDDFT calculations have been performed. Selected calculated states together with their vertical excitation energies and oscillator strengths are displayed in Table 5. The transitions under study fulfill the criteria posed by Casida [38]. The lowest in energy highly solvatochromic transition (based on experimental data) of (**1**), can be ascribed as a HOMO − 2 → LUMO transition, since the contributions from several other transitions to the final state are minor. This is in total accordance with systems described before [3] although the fragments contributions to the valence orbitals are

Table 5
Selected TDDFT calculated energies and compositions of the lowest lying singlet energy states together with oscillator strengths of (**1**)[a]

State	Composition[b]	ΔE[c]	f[d]	Character
3	HOMO − 1 → LUMO, *93%*	1.56	0.0017	W/CO → pq (MLCT/LLCT)
4	**HOMO − 2 → LUMO, *74%***	**2.09**	**0.1158**	**W/CO → pq (MLCT/LLCT)**
7	HOMO − 1 → LUMO + 1, *92%*	2.86	0.0230	W/CO → pq (MLCT/LLCT)
9	**HOMO − 2 → LUMO + 1, *56%*** **HOMO − 1 → LUMO + 2, *28%***	**2.97**	**0.0387**	**W/CO → pq (MLCT/LLCT)**
10	**HOMO − 1 → LUMO + 2, *46%*** **HOMO − 2 → LUMO + 1, *29%*** **HOMO − 2 → LUMO + 2, *14%***	**3.01**	**0.0215**	**W/CO → pq (MLCT/LLCT)**
13	HOMO − 2 → LUMO + 2, *71%* HOMO − 1 → LUMO + 2, *15%*	3.17	0.0433	W/CO → pq (MLCT/LLCT)
15	HOMO − 2 → LUMO+4, *46%* HOMO − 1 → LUMO + 3, *40%* HOMO − 1 → LUMO+4, *10%*	3.22	0.036	W/CO → CO_{ax}/W (MLCT/LLCT)
17	**HOMO − 3 → LUMO, *78%*** **HOMO − 4 → LUMO, *11%***	**3.45**	**0.0178**	**π–π* (pq)**
18	**HOMO − 4 → LUMO, *66%*** **HOMO − 3 → LUMO + 1, *11%***	**3.83**	**0.3030**	**π–π* (pq)**
20	HOMO → LUMO+6, *55%* HOMO → LUMO+8, *21%* HOMO → LUMO+5, *17%*	4.08	0.0019	W/CO_{eq} → pq (MLCT/LLCT) W/CO_{eq} → CO_{eq}/CO_{ax} (MLCT/LLCT) W/CO_{eq} → pq (MLCT/LLCT)
21	HOMO − 1 → LUMO+5, *75%* HOMO → LUMO+7, *13%*	4.13	0.0074	W/CO → pq (MLCT/LLCT) W/CO → CO_{eq}/CO_{ax} (MLCT)
22	HOMO − 1 → LUMO+7, *67%* HOMO − 2 → LUMO+4, *11%* HOMO → LUMO+6, *10%*	4.23	0.0292	W/CO → CO_{eq}/CO_{ax} (MLCT) W/L → CO_{ax}/W (MLCT/LLCT) W/CO_{eq} → pq (MLCT/LLCT)

[a] The principal singlet transition responsible for the main absorption band in the visible region is shown in bold.
[b] Compositions of electronic transitions are expressed in terms of contributing excitations between ground-state Kohn–Sham molecular orbitals.
[c] Transition energy from the a^1A_1 ground state in eV.
[d] Oscillator strength.

different since a non-symmetric ligand has been employed.

The fact that 45% from HOMO − 2′s electron density is localized on parts of the molecule other than the metal (Table 4), contradicts the widely accepted notation MLCT for this transition; it could be characterized as an oversimplification. Therefore, we adopt the term MLCT/LLCT suggested by Vlček and coworkers [39].

The HOMO − 2 → LUMO + 1 and HOMO − 1 → LUMO + 2 MLCT/LLCT transitions are responsible for the broadening of the main absorption band at the high-energy region in polar solvents (Table 5). The aforementioned transitions are perfectly distinguished in non-polar solvents e.g. hexane. Indeed the first transition is observed at 418 nm (2.97 eV) while the second at 403 nm (3.08 eV). Finally, a non-solvatochromic band at 330 nm (3.60 eV), which is experimentally observed at 332 nm (3.73 eV) is attributed to a $\pi \rightarrow \pi^*$ quinoxaline based transition.

Trying to complete the aforementioned picture regarding the solvation of the ground state and the lowest lying gas phase excited states, we employed a tandem use of TDDFT/CPCM models. The TDDFT/CPCM calculations are non-equilibrium calculations with respect to the polarization process between the solvent reaction field and the charge density of the singlet ground state [40] and they have been successfully employed in several cases during the last few years [41]. As starting geometries in this approach we selected the previously calculated ground state geometries under the influence of the solvents' field. Our results are in good agreement with the experiment with the best one being observed in the case of methanol (ΔE for the main band ~700 cm^{-1}). Our results are summarized in Fig. 6. The main feature that we observe, as it is clarified by the combined TDDFT/CPCM model, is that the ground state (S_0) faces solvent's reaction field in a larger extent, as compared to S_3 (the main UV–Vis transition of a HOMO − 2 → LUMO character, vide supra) and $\Delta E_{gs} > \Delta E_{es}$. Hence, going from the gas phase to a solution of carbon tetrachloride (a typical non-polar solvent), the ground state of the system is stabilized by 0.20 eV, with the difference being enhanced to a total value of 0.38 eV in methanol. The corresponding values in case of S_3 are 0.15 and 0.21 eV, respectively. Both S_1 (HOMO → LUMO with $f = 0.0001$) and S_2 (HOMO - 1 → LUMO with $f = 0.0017$) transitions having a negligible oscillator strength do not really affect the main band; they are not solvent depended. This situation describes the origin of the negative solvatochromism in these compounds. Thus, the main band blue shift as the solvent's electric field strengthens.

On the basis of the TDDFT results mentioned above, we could come down to the following conclusions. To begin with, the calculated energies of MLCT/LLCT

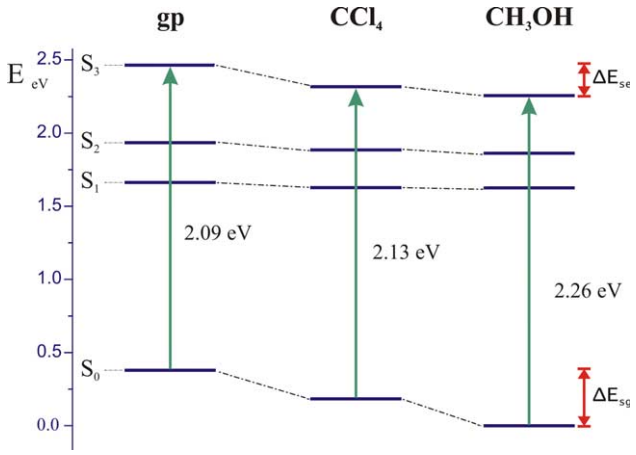

Fig. 6. Energy diagram of the lowest excited singlet states of **1** S_1(HOMO → LUMO), S_2(HOMO − 1 → LUMO) and S_3(HOMO − 2 → LUMO), in the gas phase where (first column, $E_1 = 1.28$ eV, $E_2 = 1.56$ eV, $E_3 = 2.09$ eV, for the related transitions to S_1, S_2 and S_3, respectively), in carbon tetrachloride (second column, $E_1 = 1.44$ eV, $E_2 = 1.70$ eV, $E_3 = 2.13$ eV, for the related transitions to S_1, S_2 and S_3, respectively) and methanol (third column, $E_1 = 1.63$ eV, $E_2 = 1.86$ eV, $E_3 = 2.26$ eV, for the related transitions to S_1, S_2 and S_3, respectively), as calculated by TDDFT/CPCM.

transitions are in excellent agreement to the experimental ones, considering complex's negative solvatochromism. As a matter of fact, the non-solvatochromic $\pi \rightarrow \pi^*$ quinoxaline based transition is estimated accurately. Secondly, the MO pattern calculated herein for (**1**) does not conform to the usual textbook picture of ligand-field and simple MO theories. No LF transitions were found among the lowest 21 calculated transitions in a spectroscopically relevant range up to 5 eV. All the calculated valence orbitals own a highly mixed character which reflects to their expanded delocalization; as a matter of fact no orbital of a net $d_{\sigma*}$ character has been observed. It probably exists but at a higher energy; indeed, the lowest LF transition for complexes of this class has been referenced at 5.08 eV (40,984 cm^{-1}) [3].

4.3. Solvatochromic study of (*1*)

4.3.1. Absorption spectroscopy

In consistence with other complexes of the type $M(CO)_4L$ [3b,33] (**1**) exhibits a significant negative solvatochromism taking a range of colors from pink to green (ca. 3346 cm^{-1} range) depending on the solvent. Mostly relative for the negative solvatochromism of the complex is the low energy band, whose maximum shifts to higher energies in solvents of increasing polarity. An interpretation of the solvatochromic behavior of (**1**) was attempted by a correlation of the low-energy band's maximum expressed in energy units, with the dipole moment and with the bulk dielectric constant of a variety of solvents. The values of $\tilde{\nu}$(**1**) in different solvents along with the corresponding dipole moments and dielectric constants of the solvents are displayed in Table 6.

Table 6
Maximum absorbance frequencies of MLCT transitions of (**1**) in various solvents, along with the values of dielectric constant ε and dipole moment μ of the corresponding solvents

Solvents	ε	μ (D)	$\tilde{\nu}(1)$ (cm^{-1})
Methanol	32.630	2.97	17,462
Ethanol	24.300	1.71	17,134
Acetonitrile	37.500	3.39	18,259
Acetone	20.700	3.11	17,900
THF	7.580	1.69	17,262
Chloroform	4.806	1.11	16,566
Carbon tetrachloride	2.238	0.00	15,692
Dmso	46.680	3.90	18,461
Toluene	2.438	0.37	16,557
Dmf	36.710	3.82	18,337
Diethylether	4.335	1.23	16,576
Dichloromethane	9.100	1.90	17,056
n-Heptane	1.920	0.00	15,473
Iso-octane	1.940	0.00	15,489
Acetic acid	6.150	–	16,940
Cyclohexanone	18.300	3.07	17,554
Benzene	2.284	0.00	16,750
m-Xylene	2.374	–	16,570
Piperidine	5.800	1.19	16,920
Methylethylketone	18.510	2.78	17,720
3-Pentanone	17.000	2.72	17,604
Methylisobutylketone	13.110	–	17,438
Carbon disulfide	2.641	0.00	15,703
n-Hexane	1.890	0.08	15,448
Nitromethane	35.870	3.46	18,203

Fig. 7 indicates the linear correlation between the $\tilde{\nu}$ of (**1**) and the solvent dipole moment μ; an excellent correlation coefficient is found ($r = 0.98$), which denotes the contribution of the dipolar interactions to the solvatochromic behavior of these complexes [30,42]. The negative solvatochromism of these complexes can be attributed not only to the preferential stabilization of their polar ground state, but also to the destabilization of the less polar excited state in the polar solvents. According to the Franck–Condon principle, the latter can be explained by considering that the solvent shell

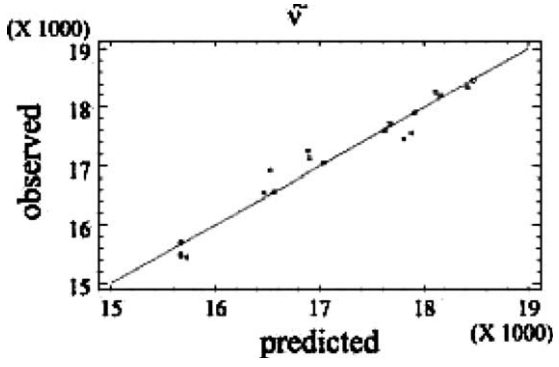

Fig. 7. Interpretation of the calculated vs. observed transition energies for $\tilde{\nu}$(**1**) according to the correlation with the dipole moments μ of the solvents ($R^2 = 0.96$), after omitting the data for the aromatic solvents.

is approximately "frozen" relative to the timeframe of the electronic excitation. As a consequence, the large dipole moments of the polar solvents, being unable to reorient after the photo-excitation, are oriented incorrectly with respect to the transition charge distribution of the complex, whose excited state becomes destabilized.

On the other hand, the data in Table 7 and in Fig. 8 reveal that, even though the overall linear fit of $\tilde{\nu}$(**1**) to ε is rather unsuccessful, acceptable linear fit patterns are taken after the segregation of the solvents into separate groups. Among the solvents we have used in our study, we can distinguish a group containing solvents with low dielectric constants (non-polar solvents) ($R = 0.944$), a group basically consisted by keto- solvents ($R = 0.975$) and finally a group, where polar, quite nucleophilic solvents are included ($R = 0.884$). On the other hand, the classification of the aromatic solvents into any of the above-mentioned groups also seems to fail, as the standard deviation of the linear correlations increases drastically. This practically means that the aromatic solvents should form a group of their own, as a result of the anisotropic effect that they impose on solute' s properties. The latter could be ascribed in part to a $\pi-\pi$ interaction of the aromatic cloud of 2,2′-pq with the solvent's one; an interaction different from any other group of solvents.

The coexistence of solvents with not only acidic but also basic character in the third group, implies that there should be no significant influence from the donor/acceptor properties of the solvents on the position of the low-energy band of (**1**). If a discrimination of the two classes of solvents had taken place a different solvation mechanism related to basic or acidic character of (**1**) would be suggested. This conclusion is further verified by the application of Kamlet–Taft scale [43], where it can be easily checked that the contribution of the acidic and basic term is trivial (p value for the acidic term >0.3, p value for the basic term >0.1) (Suppl. 1).

Another point of interest is that, although the slopes of the plots in the second and third group of solvents are similar (Fig. 7), they differ substantially from that of the non-polar solvents, with the latter attaining a greater value. This indicates that the complex is particularly sensitive to the change of the solvent in the low polarity area. The poor linearity of the fit, when all the solvents are taken into account, denotes that the dielectric constant by its own fails to describe the solvent effects in an unambiguous way. This could attributed to the fact that the values of the dielectric constant of a solvent change significantly after the introduction of a solute, obtaining values that are in direct relation to the distance from the solute's surface; herein the values for the pure solvents are employed.

As far as the extent of (**1**)'s solvatochromism is concerned, an insight can be shed by comparing it with

Table 7
The coefficients of the variable ε, the constant terms and the R of the equation $\tilde{\nu}(\mathbf{1}) = a\varepsilon + b$

		a	b	R
	All solvents	56.626	16195	0.8484
Solvent groups				
1	Dichloromethane, chloroform, carbon tetrachloride, *n*-hexane, *n*-heptane, *iso*-octane, diethylether, THF, carbon disulfide, piperidine	337.5	14882	0.9435
2	Acetone, methylisobutylketone, 3-pentanone, methylethylketone, cyclohexanone, acetic acid	62.8	16536	0.9745
3	Nitromethane, DMF, DMSO, methanol, ethanol, acetonitrile	65.9	15628	0.8837

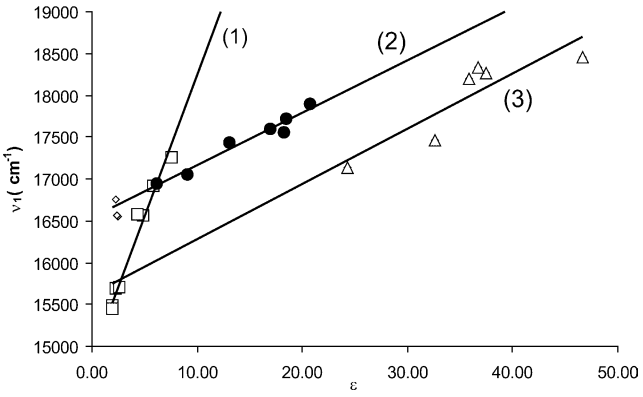

Fig. 8. Correlation diagram of $\tilde{\nu}(\mathbf{1})$ vs. the dielectric constant of the corresponding solvents. The graphical points represented as □, ●, Δ and ◇ correspond to the non-polar solvents (group 1), keto-solvents (group 2), polar, nucleophilic solvents (group 3) and the aromatic solvents.

the $W(CO)_4$phen complex; 1150 cm^{-1} is the $\Delta\tilde{\nu}$ for (**1**) going from acetone to benzene, while the corresponding difference value for $W(CO)_4$phen is 1917 cm^{-1}. We have already mentioned in the previous session that the overall electronic pattern of the tetracarbonyl α-diimine d^6 complexes is almost the same, with differences in the fragments' contribution to the energy states. The latter reflects to the extent of π-back donation. Moreover, back-donation has been accepted as one of the factors that influence the extent of solvatochromism. Hence it is obvious that the higher back-donation to 2,2′-pq (0,054 e^-) than the one to phen (0,022 e^-), fits with the smaller solvatochromism of (**1**). Apart from any electronic reasons, the size of the transition dipole moment of the complexes after their photo-excitation should be consistent with their geometrical features, among which the axial carbonyls' dihedral angle in asymmetrical (**1**) should be of considerable importance.

4.3.2. ^1H NMR spectroscopy

In Table 8 the proton chemical shifts of **2,2′-pq** and (**1**), in a number of solvents, are reported. The assignment of the peaks that correspond to the nine protons of each molecule is based on COSY experiments (Suppl. 2). Thus, it has been found that the two most deshielded protons for both 2,2′-pq and (**1**) are H_3 and H'_6; this is mainly due to the magnetic anisotropies of the Ns.

Table 8
Proton chemical shifts of **2,2′-pq** and (**1**) in various solvents

		H_3	$H_{6'}$	$H_{3'}$	H_5	H_8	$H_{4'}$	H_6	H_7	H'_5
Acet	pq	9.96	8.81	8.64	8.18	8.13	8.05	7.90	7.88	7.56
	1	10.03	9.52	9.09	8.29	9.24	8.38	8.13	8.10	7.84
DMSO	pq	9.79	8.76	8.48	8.17	8.11	8.04	7.89	7.87	7.56
	1	10.08	9.36	9.13	8.30	9.05	8.36	8.14	8.09	7.81
DMF	pq	9.95	8.84	8.61	8.19	8.14	8.11	7.95	7.92	7.61
	1	10.19	9.50	9.25	8.32	9.20	8.45	8.19	8.14	7.91
CCl_4	pq	9.97	8.74	8.64	8.14	8.08	7.86	7.74	7.71	7.36
	1	9.52	9.67	8.52	8.23	9.36	8.07	8.06	8.00	7.53
$CDCl_3$	pq	9.98	8.80	8.62	8.19	8.18	7.92	7.82	7.79	7.43
	1	9.59	9.56	8.52	8.26	9.32	8.13	8.04	8.00	7.55
CD_2Cl_2	pq	9.95	8.77	8.61	8.17	8.13	7.93	7.81	7.79	7.43
	1	9.63	9.51	8.54	8.25	9.27	8.13	8.04	8.00	7.57
CD_3CN	pq	9.92	8.79	8.59	8.17	8.13	8.01	7.87	7.84	7.52
	1	9.75	9.44	8.74	8.26	9.19	8.23	8.07	8.04	7.67
CD_3OD	pq	9.85	8.77	8.60	8.19	8.13	8.02	7.89	7.86	7.53
	1	9.87	9.49	8.91	8.28	9.27	8.26	8.06	8.05	7.70

The proton that resonates next is H'_3 for 2,2′-pq and H_8 for (**1**). This difference stems from the fact that H'_3 in the free ligand may interact through space with N_1 of the opposed aromatic ring and as a consequence it deshields. The aforementioned interaction is lost after complexation because of the twisting of the pyridyl moiety of 2,2′-pq around the C_2–C'_2 bond so as N_1 and N'_3 bind with W [29,44]. On the other hand, after the complexation a novel interaction through space between H_3 and H'_3 is established, which is depicted in NOESY experiments of (**1**) (Fig. 9). The geometrical change of the ligand, along with the change of the electronic distribution on it, after its coordination to W, results in an overall downfield shift of the protons, which is particularly pronounced for H_8 (Table 8).

When considering the effects of different solvents on ^{1}H chemical shifts, it is important to distinguish between intrinsic solvent effects and those which occur as a result of a change in the solute conformation or structure due to the change in solvent. The intrinsic solvent effect may be attributed to the different anisotropy, polarity or polarizability of the solvents, while the specific solvent effects may be due to polarity changes and chemical effects, in particular hydrogen bonding.

As it is seen in Table 8, the proton chemical shifts of 2,2′-pq change with the solvent – the highest difference recorded is 0.25 ppm between CCl_4 and d_7-dmf. The chemical shift differences for each proton of the molecule are not the same reflecting at the same time the intrinsic and the specific solute–solvent interactions. The general trend is a low-field shift on moving to more polar solvents for all protons except from H_3 and H'_3. Due to their location in the molecule, these two protons

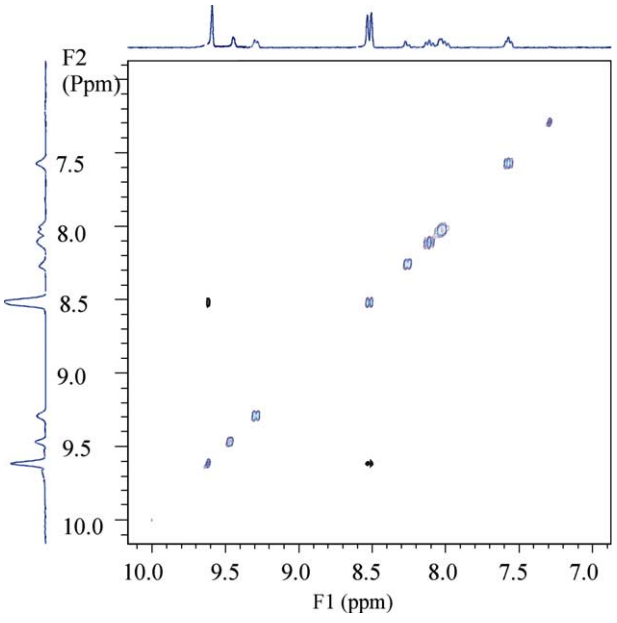

Fig. 9. NOESY spectrum of (**1**) in $(CD_3)_2CO$.

are the most influenced by the relative direction of the quinoxaline in relation to the pyridine ring moiety; even a small twist of the pyridine around the bond C_2–C'_2 could directly affect these protons' chemical shifts. The anomalous trend that these two protons exhibit as the solvent polarity changes can be assigned as an intramolecular structural change – a ring twist, in particular. The latter is the consequence of the effect that some solvents impose on solute's structure and the value of the twist-angle should depend on the solvent.

As far as (**1**) is concerned, the solvent change seems to affect its proton chemical shifts more than the ones of the free ligand (Table 8), as it has been previously reported for analogous diimines and their complexes [45]. The ^{1}H NMR spectra of (**1**) in various solvents are schematically presented in Fig. 10. The recorded maximum shifts correspond to H'_3 and then to H_3 and can be up to 0.7 ppm (CCl_4 to d_7-dmf). In contrast to 2,2′-pq, all complex's shifts are mainly affected by solvents' intrinsic effects as no change in the dihedral angle of the two heterocyclic ring planes of the bidentate ligand is expected. In accordance to the rigidity of the ligand in the complex the chemical shifts of (**1**) correlate with the polarity of the solvents – expressed by their dipole moments – in contradiction to the free ligand's shifts.

It is straight forward to verify that the observed chemical shifts of (**1**) are in consistence with the Mülliken atomic partial charges in solvents with different polarity, e.g. CCl_4 and MeOH (Table 9). On the one hand, there is an overall, gradual proton deshielding in (**1**) when the solvents become more polar – a trend only disturbed by the shielding of H'_6 and H_8 to the more polar solvents. On the other hand, Mülliken values indicate a general increase in the positive charges of the protons, in parallel to the increase of solvent cage's polarity. As a matter of fact, the transition from CCl_4 to MeOH signifies a charge transfer from the axial COs and the central metal to the equatorial COs and the internal nuclei of 2,2′-pq. Nevertheless, it was interesting to observe an increase of the positive charge on C_2–C'_2 and a slight decrease of the negative charge of N_1. The highest atomic partial charge difference is predicted for H'_3 in accordance with the experimentally observed ^{1}H-shifts in these two solvents. Finally, the anomalous trend of H_8 is predicted by the Mülliken analysis; a decrease of positive charge in MeOH correlates with its shielding in the polar solvents.

The solvent effect on H'_6 and H_8, named shielding in the polar solvents, could be attributed to their location in the molecule, in a region very susceptible to the magnetic anisotropy of the CO ligands. In other words H'_6 and H_8 being remote and protected from direct contact with solvent molecules, could be affected by any perturbation in electronic population on COs, caused by solvents.

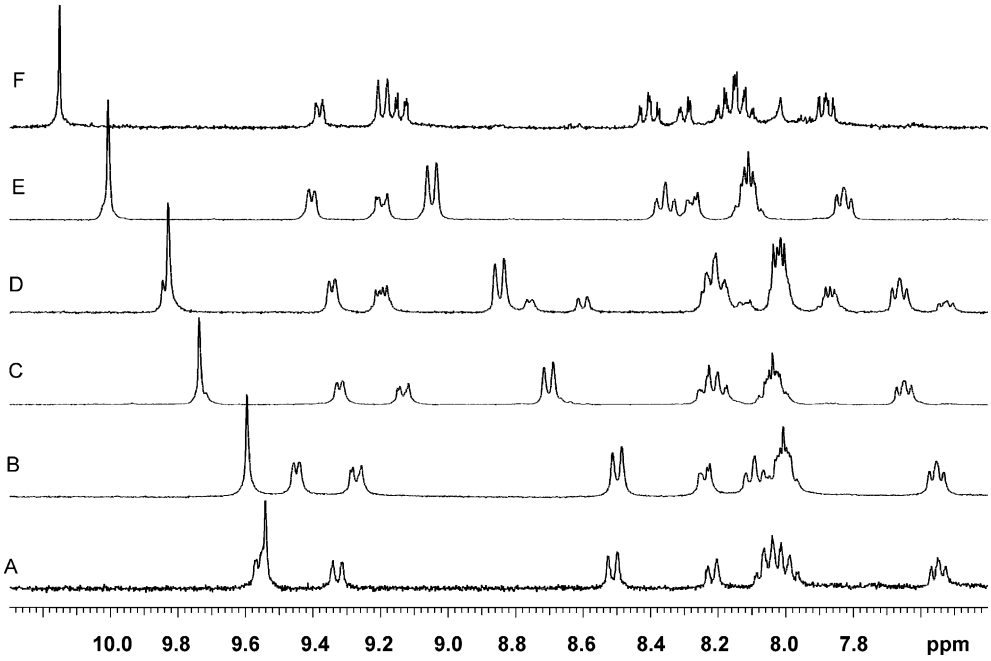

Fig. 10. Mülliken atomic partial charges of (**1**) in CCl_4 and MeOH.

Table 9
Mülliken charges for the ground state structures

Atom	Gas phase	CCl_4	CH_3OH
W	+0.751	+0.756	+0.763
N1	−0.290	−0.290	−0.286
N1′	−0.306	−0.306	−0.307
C2	+0.312	+0.320	+0.338
C2′	+0.225	+0.229	+0.238
C11	−0.082	−0.086	−0.088
O1	−0.182	−0.198	−0.231
C14	−0.085	−0.093	−0.104
O4	−0.182	−0.201	−0.240
C12	−0.057	−0.055	−0.048
O2	−0.139	−0.153	−0.177
C13	−0.057	−0.055	−0.048
O3	−0.139	−0.153	−0.177
N4	+0.025	+0.015	−0.019
H6	0.2393	0.2491	0.2714
H5	0.2642	0.2699	0.2909
H7	0.2440	0.2501	0.2695
H8	0.2714	0.2672	0.2645
H3	0.2388	0.2536	0.2929
H3′	0.2329	0.2497	0.2980
H4′	0.2487	0.2652	0.3063
H6′	0.2769	0.2763	0.3020
H5′	0.2460	0.2605	0.2987

A reasonable question that could be raised is whether and how the negative solvatochromic behavior of the tetracarbonyl α-diimine d^6 complex is interpreted by ^1H NMR spectroscopy. As we have already noted, HOMO − 2 not only has a key importance to the solvatochromism of the complexes of this series but also it is indicative of the extent of back-donation process. As a whole, the delocalization of electron density on diimine at the ground state reduces the extent of the observed solvatochromism. Besides, one should expect an enhanced contribution of diimine's orbitals to the ground state to nominate high solvent-induced chemical shifts. On the basis of the aforementioned arguments and on experimental and theoretical results both herein and in the literature [3,45], we deduce that the most solvatochromic is a diimine-tetracarbonyl complex, the smallest shielding of diimine's ^1H shifts is induced by changing the solvent.

5. Conclusions

In this work, we present the synthesis, characterization and crystallographic data of the novel complex $W(CO)_4$(2,2′-pq) (**1**). The character of its ground state and the way that the orbitals of $W(CO)_4$ moiety interact with those of 2,2′-pq, so as to form the orbitals of (**1**) are investigated by means of DFT calculations. On the other hand, an important property of (**1**), that is its negative solvatochromism, is examined through absorption and NMR spectroscopy, while TDDFT calculations reveal the electronic transition that entails its major solvatochromic character. Moreover, DFT calculations using solvent cages depict the solvents' influence on complex's energy levels. The influence of the solvents on (**1**)'s properties does not seem to arise either from an acid/base interaction or an induced structural transformation, but it is more likely to originate from a significant charge redistribution on (**1**) depending on the solvent. As a matter of fact, our DFT calculations

indicated that the polar solvents enhance the $(CO)_{eq}$'s and diimine's contribution in HOMO and LUMO, respectively. The mixing of frontier orbitals, the amount of back-bonding and some factors related to complexes' structure and asymmetry must be taken in account for the interpretation of the solvatochromism's extent in a series of complexes analogous to (**1**).

Acknowledgments

We thank the Special Research Account of Athens University for partial support. Appreciation is expressed to Serge Gorelsky for discussions on the AOMix-CDA capabilities and to A. Vlček for the fruitful discussions.

Appendix A. Supplementary data

Crystallographic data for the structural analysis has been deposit with the Cambridge Crystallographic data Centre, CCDC Nos. 268254 for compound $W(CO)_4$-(2,2′-pq). Copies of this information may be obtained free of charge from: deposit@ccdc.cam.ac.uk or www: http://www.ccdc.cam.ac.uk. Supplementary data associated with this article can be found, in the online version, at doi:10.1016/j.jorganchem.2005.07.023.

References

[1] F.A. Cotton, G. Wilkinson, Advanced Inorganic Chemistry, fifth ed., Wiley-Interscience, New York, 1988.
[2] D.J. Stufkens, Coord. Chem. Rev. 104 (1990) 39.
[3] (a) A. Vlček Jr., Coord. Chem. Rev. 230 (2002) 225;
(b) I.R. Farrel, H. Františ ek, S. Záliš, T. Mahabiersing, A. Vlček Jr., J. Chem. Soc. Dalton Trans. (2000) 4323;
(c) I.R. Farrel, J. van Slageren, S. Záliš, A. Vlček Jr., Inorg. Chim. Acta 315 (2001) 44;
(d) S. Záliš, I.R. Farrel, A. Vlček Jr., J. Am. Chem. Soc. 125 (2003) 4580;
(e) S. Záliš, M. Busby, T. Kotrba, P. Matousek, M. Towrie, A. Vlček Jr., Inorg. Chem. 43 (2004) 1723.
[4] A.J. Lees, Coord. Chem. Rev. 177 (1998) 3.
[5] (a) D.R.Van Staveren, N. Metzler-Nolte, Chem. Commun. (2002) 1406;
(b) N. Metzler-Nolte, Angew. Chem., Int. Ed. 40 (2001) 1040.
[6] V. Balzani, A. Juris, M. Venturi, S. Campagna, S. Serroni, Chem. Rev. 96 (1996) 759.
[7] (a) D.R. Kanis, M.A. Ratner, T.J. Marks, J. Am. Chem. Soc. 112 (1990) 8203;
(b) J. Messier, F. Kajar, P. Prasad, D. (Eds.), Ulrich, Nonlinear Optical Effects in Organic Polymers, Kluwer Academic Publishers, Dordrecht, 1989;
(c) D.J. Williams, Angew. Chem., Int. Ed. Engl. 23 (1984) 690.
[8] L. Onsager, J. Am. Chem. Soc. 58 (1936) 1486.
[9] M.G. Knize, C.P. Salmon, E.C. Hopmans, et al., J. Chromatogr. A 763 (1–2) (1997) 179.
[10] (a) N.E. Mollegaard, C. Bailly, M.J. Waring, P.E. Nielsen, Biochemistry 39 (2000) 9502;
(b) H.-R. Park, T.H. Kim, K.-M. Bark, Eur. J. Med. Chem. (2002) 1.
[11] (a) M. Inoue, M. Kubo, Coord. Chem. Rev. 21 (1976) 1;
(b) Z. Kucybala, I. Pyszka, J. Paczkowski, J. Chem. Soc., Perkin Trans. 2 (2000) 1559.
[12] (a) W. Kaim, Angew. Chem., Int. Ed. Engl. 22 (1983) 171;
(b) R. Czerwieniec, J. Herbich, A. Kapturkiewicz, J. Nowacki, Chem. Phys. Lett. 325 (2000) 589.
[13] (a) C. Lauterbach, J. Fabian, Eur. J. Inorg. Chem. (1999) 1995;
(b) D.V. Fomitchev, B.S. Lim, R.H. Holm, Inorg. Chem. 40 (2001) 645;
(c) D. Herebian, K.E. Wieghardt, F. Neese, J. Am. Chem. Soc. 125 (2003) 10997;
(d) A. Rosa, E.J. Baerends, S.J.A. van Gisbergen, E. van Lenthe, J.A. Groeneveld, J.G. Snijders, J. Am. Chem. Soc. 121 (1999) 10356;
(e) S.R. Stoyanov, J.M. Villegas, D.P. Rillema, J. Phys. Chem. B. 108 (2004) 12175;
(f) S. Curreli, P. Deplano, C. Faulmann, A. Ienco, C. Mealli, M.L. Mercuri, L. Pilia, G. Pintus, A. Serpe, E.F. Trogu, Inorg. Chem. 43 (2004) 5069.
[14] S. Kasselouri, A. Garoufis, A. Katehanakis, G. Kalkanis, S.P. Perlepes, N. Hadjiliadis, Inorg. Chim. Acta 207 (1993) 255.
[15] D.D. Perrin, W.L.F. Armarego, Purification of Laboratory Chemicals, third ed., Pergamon Press, New York, 1988.
[16] G.M. Sheldrick, SHELXS-97, Program for the Structure Solution, SHELXL-97, Program for the Refinement of Crystal Structures, University of Gottingen, Gottingen, Germany, 1997.
[17] L.J. Farrugia, J. Appl. Cryst. 30 (1997) 565.
[18] R.G. Parr, W. Yang, Density Functional Theory of Atoms and Molecules, Oxford University Press, Oxford, 1989.
[19] M.J. Frisch, G.W. Trucks, H.B. Schlegel, G.E. Scuseria, M.A. Robb, J.R. Cheeseman, V.G. Zakrzewski, J.A. Montgomery Jr., R.E. Stratmann, J.C. Burant, S. Dapprich, J.M. Millam, A.D. Daniels, K.N. Kudin, M.C. Strain, O. Farkas, J. Tomasi, V. Barone, M. Cossi, R. Cammi, B. Mennucci, C. Pomelli, C. Adamo, S. Clifford, J. Ochterski, G.A. Petersson, P.Y. Ayala, Q. Cui, K. Morokuma, D.K. Malick, A.D. Rabuck, K. Raghavachari, J.B. Foresman, J. Cioslowski, J.V. Ortiz, A.G. Baboul, B.B. Stefanov, G. Liu, A. Liashenko, P. Piskorz, I. Komaromi, R. Gomperts, R.L. Martin, D.J. Fox, T. Keith, M.A. Al-Laham, C.Y. Peng, A. Nanayakkara, M. Challacombe, P.M.W. Gill, B. Johnson, W. Chen, M.W. Wong, J.L. Andres, C. Gonzalez, M. Head-Gordon, E.S. Replogle, J.A. Pople, GAUSSIAN-98. Revision A.9, Gaussian Inc., Pittsburgh, PA, 1998.
[20] A.D. Becke, J. Chem. Phys. 98 (1993) 5648.
[21] C. Lee, W. Yang, R.G. Parr, Phys. Rev. B 37 (1988) 785.
[22] (a) T.H. Dunning Jr., P.J. Hay, in: H.F. SchaeferIII (Ed.), Modern Theoretical Chemistry, vol. 3, Plenum Press, New York, 1976;
(b) P.J. Hay, W.R. Wadt, J. Chem. Phys. 82 (1985) 270.
[23] (a) V. Barone, M. Cossi, J. Phys. Chem. A 102 (1998) 1995;
(b) M. Cossi, N. Rega, G. Scalmani, V. Barone, J. Comp. Chem. 24 (2003) 669.
[24] (a) S.I. Gorelsky AOMix progam, revision 5.95 and AOMix-CDA, revision 1.7. Available from: http://www.sg-chem.net/;
(b) S.I. Gorelsky, A.B.P. Lever, J. Organomet. Chem. 635 (2001) 187.
[25] (a) R. Stratmann, G. Scuseria, M. Frisch, J. Chem. Phys. 109 (1998) 8218;
(b) M.E. Casida, C. Jamorski, K.C. Casida, D.R. Salahub, J. Chem. Phys. 108 (1998) 4439.
[26] M.J. Frisch, G.W. Trucks, H.B. Schlegel, G.E. Scuseria, M.A. Robb, J.R. Cheeseman, J.A. Montgomery Jr., T. Vreven, K.N. Kudin, J.C. Burant, J.M. Millam, S.S. Iyengar, J. Tomasi, V. Barone, B. Mennucci, M. Cossi, G. Scalmani, N. Rega, G.A. Petersson, H. Nakatsuji, M. Hada, M. Ehara, K. Toyota, R. Fukuda, J. Hasegawa, M. Ishida, T. Nakajima, Y. Honda, O. Kitao, H. Nakai, M. Klene, X. Li, J.E. Knox, H.P. Hratchian,

J.B. Cross, C. Adamo, J. Jaramillo, R. Gomperts, R.E. Stratmann, O. Yazyev, A.J. Austin, R. Cammi, C. Pomelli, J.W. Ochterski, P.Y. Ayala, K. Morokuma, G.A. Voth, P. Salvador, J.J. Dannenberg, V.G. Zakrzewski, S. Dapprich, A.D. Daniels, M.C. Strain, O. Farkas, D.K. Malick, A.D. Rabuck, K. Raghavachari, J.B. Foresman, J.V. Ortiz, Q. Cui, A.G. Baboul, S. Clifford, J. Cioslowski, B.B. Stefanov, G. Liu, A. Liashenko, P. Piskorz, I. Komaromi, R.L. Martin, D.J. Fox, T. Keith, M.A. Al-Laham, C.Y. Peng, A. Nanayakkara, M. Challacombe, P.M.W. Gill, B. Johnson, W. Chen, M.W. Wong, C. Gonzalez, J.A. Pople, GAUSSIAN-03, Revision A.1, Gaussian, Inc., Pittsburgh, PA, 2003.

[27] S.I. Gorelsky, SWizard program. Available from: http://www.sgchem.net/.

[28] W. Strohmeier, F.J. Müller, Chem. Ber. 102 (1969) 3608.

[29] S. Kasselouri, A. Garoufis, S. Paschalidou, S.P. Perlepes, I.S. Butler, N. Hadjiliadis, Inorg. Chim. Acta 227 (1994) 129.

[30] I. Veroni, A. Rontoyianni, C.A. Mitsopoulou, J. Chem. Soc., Dalton Trans. (2003) 255.

[31] (a) E.G. Bakalbassis, J. Mrozinski, S.P. Perlepes, N. Hadjiliadis, F. Lianza, A. Albinati, Polyhedron 13 (1994) 3209;
(b) A. Garoufis, A. Koutsodimou, C.P. Raptopoulou, A. Simopoulos, N. Katsaros, Polyhedron 18 (1999) 3005.

[32] (a) D.J. Darensbourg, J.D. Draper, B.J. Frost, J.H. Reibenspies, Inorg. Chem. 38 (1999) 4705;
(b) C.-H. Ueng, G.-Y. Shih, Acta Cryst. C 48 (1992) 988;
(c) R. Hage, R.A.G. De Graaff, J.G. Haasnoot, Acta Cryst. C 47 (1991) 2448;
(d) P.-Y. Yang, F.-C. Chang, M.-C. Suen, J.-D. Chen, T.-C. Keng, J.-C. Wang, J. Organomet. Chem. 596 (2000) 226.

[33] (a) J. Chatt, H.R. Watson, J. Chem. Soc. (1961) 4980;
(b) C.S. Kraihanzel, F.A. Cotton, Inorg. Chem. 2 (1963) 533;
(c) L.E. Orgel, Inorg. Chem. 1 (1962) 25;
(d) D.M. Manuta, A.J. Lees, Inorg. Chem. 25 (1986) 1354.

[34] D.M. Manuta, A.J. Lees, Inorg. Chem. 22 (1983) 3825.

[35] (a) A.E. Reed, L.A. Curtiss, F. Weinhold, Chem. Rev. 88 (1988) 899;
(b) E.D. Glendening, A.E. Reed, J.E. Carpenter, F. Weinhold, NBO Version 3.1;
(c) S. Dapprich, G. Frenking, J. Chem. Phys. 99 (1995) 9352;
(d) G. Frenking, N. Fröhlich, Chem. Rev. 100 (2000) 717.

[36] R. Stowasser, R. Hoffmann, J. Am. Chem. Soc. 121 (1999) 3414.

[37] C. Makedonas, C.-A. Mitsopoulou, F.J. Lahoz, A.I. Balana, Inorg. Chem. 83 (2003) 6336.

[38] M.E. Casida, C. Jamorski, K.C. Casida, D.R.J. Salahub, Chem. Phys. 108 (1998) 4439.

[39] I.R. Farrell, A. Vlček, Coord. Chem. Rev. 208 (2000) 87.

[40] AE. Frisch, M.J. Frisch, G.W. Trucks, GAUSSIAN-03 User's Refernce, version 7.0, Gaussian, Inc., Carnegie, PA, 2003, p. 206.

[41] (a) J.M. Villegas, S.R. Stoyanov, W. Huang, D.P. Rillema, Inorg. Chem. 44 (2005) 2297;
(b) J.M. Villegas, S.R. Stoyanov, W. Huang, D.P. Rillema, Dalton Trans. (2005) 1042;
(c) J.M. Villegas, S.R. Stoyanov, J.H. Reibenspies, D.P. Rillema, Organometallics 44 (2005) 395;
(d) S.R. Stoyanov, J.M. Villegas, A.J. Cruz, L.L. Lockyear, J.H. Reibenspies, D.P. Rillema, J. Chem. Theory Comput. 1 (2005) 95;
(e) J.-F. Guillemoles, V. Barone, L. Joubert, C. Adamo, J. Phys. Chem. A 106 (2002) 11345;
(f) V. Barone, F.F. de Biani, E. Ruiz, B. Sieklncka, J. Am. Chem. Soc. 123 (2001) 10742.

[42] (a) H. Saito, J. Fujita, K. Saito, Bull. Chem. Soc. Jpn. 41 (1968) 863;
(b) E.S. Dodsworth, A.B.P. Lever, Inorg. Chem. 29 (1990) 499.

[43] M.J. Kamlet, J.-L.M. Abboud, M.H. Abraham, R.W. Taft, J. Org. Chem. 48 (1983) 2877.

[44] S. Castellano, H. Gunther, S. Ebersole, J. Phys. Chem. 69 (1965) 4166.

[45] J.A. Connor, C. Overton, J. Organomet. Chem. 282 (1985) 349.